

# Defect-Free Erbium Silicide Formation Using an Ultrathin Ni Interlayer

Juyun Choi,<sup>†</sup> Seongheum Choi,<sup>†</sup> Yu-Seon Kang,<sup>‡</sup> Sekwon Na,<sup>†</sup> Hoo-Jeong Lee,<sup>†</sup> Mann-Ho Cho,<sup>‡</sup> and Hyoungsub Kim<sup>\*†</sup>

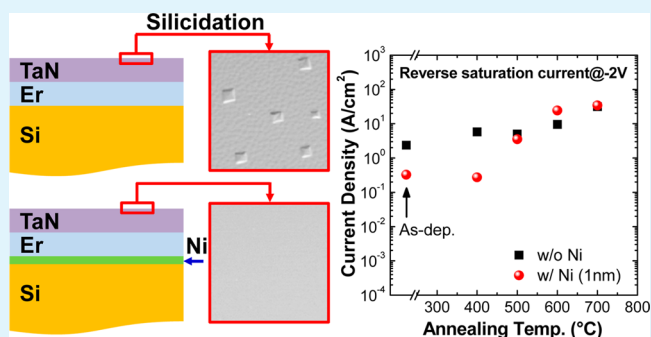
<sup>†</sup>School of Advanced Materials Science and Engineering, Sungkyunkwan University, Suwon 440-746, Republic of Korea

<sup>‡</sup>Institute of Physics and Applied Physics, Yonsei University, Seoul 120-749, Republic of Korea

## Supporting Information

**ABSTRACT:** An ultrathin Ni interlayer ( $\sim 1$  nm) was introduced between a TaN-capped Er film and a Si substrate to prevent the formation of surface defects during thermal Er silicidation. A nickel silicide interfacial layer formed at low temperatures and incurred uniform nucleation and the growth of a subsequently formed erbium silicide film, effectively inhibiting the generation of recessed-type surface defects and improving the surface roughness. As a side effect, the complete transformation of Er to erbium silicide was somewhat delayed, and the electrical contact property at low annealing temperatures was dominated by the nickel silicide phase with a high Schottky barrier height. After high-temperature annealing, the early-formed interfacial layer interacted with the growing erbium silicide, presumably forming an erbium silicide-rich Er–Si–Ni mixture. As a result, the electrical contact property reverted to that of the low-resistive erbium silicide/Si contact case, which warrants a promising source/drain contact application for future high-performance metal–oxide–semiconductor field-effect transistors.

**KEYWORDS:** Er, Ni, silicide, interlayer, surface defect, TaN



## 1. INTRODUCTION

Erbium has been acknowledged as a promising silicide-forming metal due to the low Schottky barrier height ( $\sim 0.28$  eV)<sup>1</sup> and contact resistivity ( $\sim 8.0 \times 10^{-10} \Omega \text{ cm}^2$ )<sup>2</sup> of its silicide form (ErSi<sub>2-x</sub>) on n-type Si. These aspects are beneficial to the fabrication of source/drain contacts for metal–oxide–semiconductor field-effect transistors (MOSFETs) and Schottky barrier MOSFETs, though thermally induced Er–Si reaction (silicidation) technology warrants further study to resolve inherent problems before it can successfully replace conventional contact materials such as titanium, cobalt, and nickel silicides. Because Er is prone to oxidation during the thermal annealing process, the introduction of an oxygen-blocking capping layer is mandatory, and various materials have been suggested.<sup>1,3–10</sup> Another obstacle is the generation of surface defects in either recessed or protruding shapes, depending on the process conditions.<sup>8–10</sup> In our previous study,<sup>10</sup> we were able to minimize the formation of erbium silicate and eliminate protruding pyramidal defects by adopting a TaN capping film approximately 20 nm in thickness as an oxygen-blocking layer. However, this method was not successful in removing recessed defects (pitlike and square/rectangular-shaped defects), which are believed to originate from the nonuniform island formation of crystalline ErSi<sub>2-x</sub> and the localized Si out-diffusion occurring

at the Er/Si interface region during an early silicide-forming stage.<sup>5,9,10</sup>

In this study, we propose to remove these remnant recessed defects by introducing an ultrathin Ni interlayer ( $\sim 1$  nm) between the TaN-capped Er film and the Si substrate. Ni is known to form a laterally uniform nickel silicide film at relatively low temperatures via the Ni diffusion-controlled growth mechanism,<sup>11,12</sup> while ErSi<sub>2-x</sub> forms at a slightly higher temperature ( $\sim 400$  °C) via Si diffusion, following a nucleation-controlled mechanism.<sup>13</sup> We anticipate the initiation of uniform nucleation of the ErSi<sub>2-x</sub> layer on the surface of the preformed nickel silicide layer. On the basis of diverse characterization results, the removal of recessed surface defects by the Ni interlayer is confirmed, and detailed information on the silicidation mechanism of an Er/Ni/Si system is suggested. Finally, the impact of the Ni interlayer on the electrical contact property of erbium silicide/Si is examined.

## 2. EXPERIMENTAL SECTION

n-type Si(100) substrates with a resistivity of 6–7  $\Omega \cdot \text{cm}$  were ultrasonically cleaned for 5 min each with a series of acetone, methanol, and deionized water, followed by dipping in a buffered oxide

Received: June 26, 2014

Accepted: August 5, 2014

Published: August 5, 2014

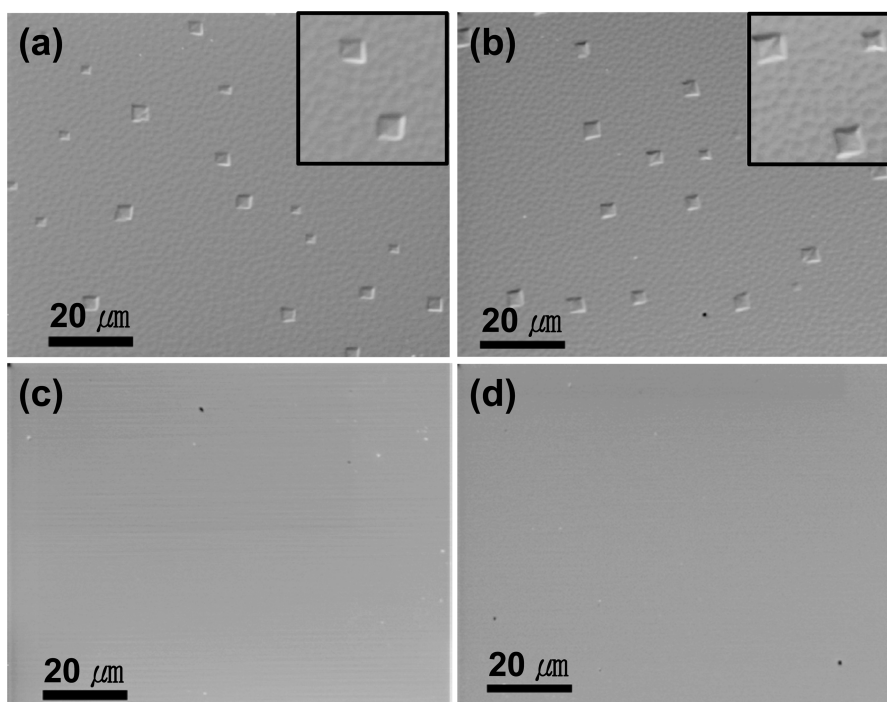


**Figure 1.** SAM surface images of the TaN/Er/Si samples (a, b) without and (c, d) with a  $\sim 1$  nm thick Ni interlayer after annealing at different temperatures: (a, c) 500 °C and (b, d) 600 °C. The insets of (a) and (b) are the corresponding high-magnification images disclosing the existence of both recessed pits and square defects.

etchant (BOE) to remove the native oxide. The samples were then immediately loaded into a load-lock chamber to minimize further surface contamination. Subsequent metal depositions were carried out in situ using a dc magnetron sputtering system maintained at a base pressure of  $\sim 2.5 \times 10^{-7}$  Torr. All metal films were sputter-deposited at a working pressure and power of  $\sim 4$  mTorr and 30 W, respectively, with the exception of Ni, which was deposited at a power of 100 W. A Ni film approximately 1 nm in thickness was used as an interlayer (using a sputtering target with a purity of 99.99%), and an Er film approximately 29 nm in thickness was subsequently deposited on top (using a sputtering target with a purity of 99.95%). As reference samples, pure Er and Ni films with a thickness of approximately 30 nm were deposited directly onto Si. Following the Er deposition, all samples were capped by an oxidation-preventing TaN film (a sputtering target purity of 99.5%) with a thickness of  $\sim 50$  nm, sufficient enough to block oxygen incorporation into the underlying Er film.<sup>10</sup> After the metal deposition, all samples were annealed with a rapid thermal processor at varying temperatures (300–700 °C) for 1 min while being maintained at a constant pressure of  $\sim 1$  Torr with a high-purity  $N_2$  (99.999%) flow.

The temperature-dependent silicidation process was examined via X-ray diffractometry (XRD; PANalytical, X<sup>2</sup>pert PRO-XRD) with Cu  $K\alpha$  radiation. In-depth information on the chemical change near the Ni interlayer was obtained via X-ray photoelectron spectroscopy (XPS; Physical Electronics, Inc., PHI5000 versa probe) using a monochromatic Al  $K\alpha$  X-ray source ( $h\nu = 1486.7$  eV) with a pass energy of 23.5 eV. The measured full width at half-maximum of a reference Ag 3d peak is approximately 0.45 eV, and the peak shift is distinguishable down to about 0.1 eV. A lightweight Ne ion beam with a sputtering power of 2 keV was used as an etching gas for depth profiling at a working pressure of  $\sim 1$  mPa to minimize sputtering artifacts. The surface and cross-sectional microstructures were examined via scanning Auger electron microscopy (SAM; Physical Electronics, Inc., PHI 700) and transmission electron microscopy (TEM; JEOL, JEM 2100F), respectively. In addition, the surface roughness was measured upon completion of the silicidation process using atomic force microscopy (AFM; Seiko Instruments, Inc., SPA-300HV) in noncontact mode.

To examine the electrical contact properties between a metal silicide and a Si substrate, circular patterns with a diameter of 100  $\mu\text{m}$  were fabricated via a liftoff process, as explained below. After negative photoresist (PR) patterning on a BOE-cleaned Si wafer, 1% HF cleaning for 1 min and metal deposition were conducted in series. Afterward, the circular metal patterns were defined by removing the PR in acetone. Following thermal silicidation at various temperatures, leakage current density vs voltage ( $J$ – $V$ ) characteristics were measured from two adjacent patterns using an Agilent B1500A semiconductor device analyzer.

### 3. RESULTS AND DISCUSSION

The surfaces of the annealed TaN/Er/Si samples were inspected via SAM, both with and without a Ni interlayer. Representative surface images are shown in Figure 1, taken after annealing at 500 and 600 °C. These temperatures correspond to the partial and near-complete conversion to erbium silicide of the sample without a Ni interlayer (reference sample), as verified in our previous report.<sup>10</sup> In addition to many small-sized surface pits with a high density, the reference sample possesses a number of large-sized, recessed defects of a square shape, even when exposed to an annealing temperature of 500 °C, as shown in Figure 1a,b. In contrast, samples with a Ni interlayer exhibit a clean surface free of notable defects under identical annealing conditions, as shown in Figure 1c,d. No defects were found even after annealing at 700 °C.

To further scrutinize the surface morphology, AFM measurements were performed on samples annealed at 600 °C with different scanning areas, as shown in Figure 2. Consistent with the SAM images, no surface defect was observed on the sample with the Ni interlayer (Figure 2c), whereas a number of recessed square defects were clearly identified on the reference sample (Figure 2a). Moreover, in terms of the root-mean-square (rms) surface roughness measured from the square-defect-free regions selected from both samples (see Figure

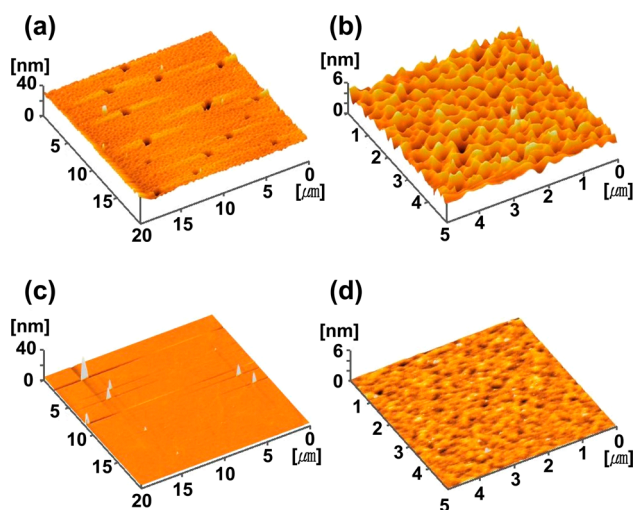


**Figure 2.** AFM surface images of the TaN/Er/Si samples (a, b) without and (c, d) with a  $\sim 1$  nm thick Ni interlayer after annealing at  $600^\circ\text{C}$  taken on different scanning areas.

2b,d), the Ni-interlayered sample resulted in a much lower value than the reference sample,  $\sim 0.06$  and  $\sim 0.75$  nm for samples with and without the Ni interlayer, respectively, within a scanning area of  $5\ \mu\text{m} \times 5\ \mu\text{m}$ . Although the rms values were obtained from the capped TaN films, it is possible to compare the surface roughness of the underlying silicide films.

As suggested in our previous study<sup>10</sup> and others,<sup>5,9</sup> the formation of recessed defects (pits and square defects) can be explained by localized Si diffusion due to the nonuniform nucleation/growth of island-shaped  $\text{ErSi}_{2-x}$  crystallites at an early Er silicidation stage. On the basis of this model, we can describe the early interfacial reaction in the Ni-interlayered sample as follows. The initial formation of a uniform, ultrathin Ni–Si reactant layer (most likely nickel silicide) via Ni diffusion-controlled growth kinetics<sup>12</sup> from an interlayered Ni film in direct contact with a Si substrate is believed to be helpful in incurring subsequent or simultaneous uniform nucleation/growth of  $\text{ErSi}_{2-x}$  and, more globally, homogeneous out-diffusion of Si atoms through the formed interfacial layer. This process may lead to a defect-free and smooth sample surface, as revealed through SAM and AFM analyses.

Although the introduction of an ultrathin Ni interlayer is proven to effectively prevent the formation of surface defects (specifically recessed defects) and reduce the surface roughness, it is necessary to verify whether the entire Er film can be completely converted to an erbium silicide film at a reasonably low temperature. The temperature-dependent silicidation reaction was investigated via XRD measurements on samples annealed at  $300$ – $700^\circ\text{C}$  with a step of  $100^\circ\text{C}$ , as shown in Figure 3. Crystalline  $\text{ErSi}_{2-x}$  peaks begin to appear in the reference sample without a Ni interlayer after annealing at a temperature over  $400^\circ\text{C}$  (Figure 3a), and a significantly large increase in intensity was observed at temperatures over  $500^\circ\text{C}$ , demonstrating a reproducible result in conjunction with our previous experiment.<sup>10</sup> No erbium oxide peaks ( $\text{ErO}_x$  or  $\text{Er}_2\text{O}_3$ ) were identified throughout the range of annealing temperatures, confirming the effective blocking of oxygen incorporation into the Er film by the  $\sim 50$  nm thick TaN capping layer. A similar evolution of XRD spectra under varying annealing temperatures was observed for the sample with the Ni interlayer (Figure 3b) compared to the reference sample without Ni. The only notable

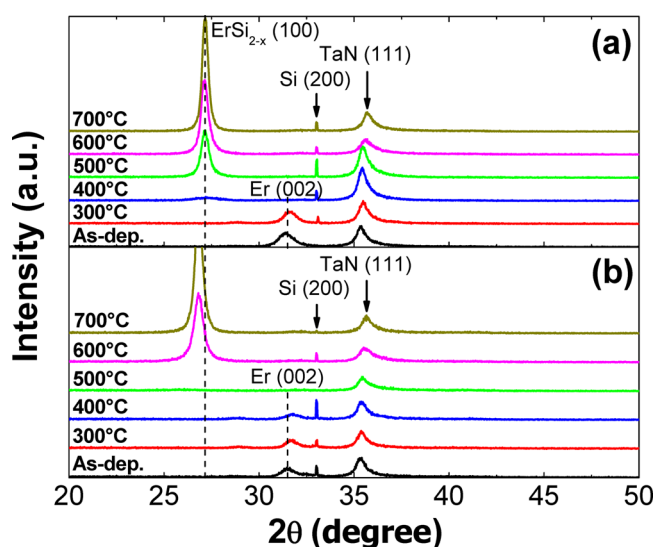


**Figure 3.** XRD spectra obtained from the TaN/Er/Si samples (a) without and (b) with a  $\sim 1$  nm thick Ni interlayer as a function of the annealing temperature, including the as-deposited states.

difference is the onset temperature of  $\text{ErSi}_{2-x}$  formation; the first hexagonal  $\text{ErSi}_{2-x}(100)$  peak appeared at an annealing temperature of  $600^\circ\text{C}$  in the Ni-interlayered sample. This implies that  $\text{ErSi}_{2-x}$  formation begins at an annealing temperature over  $500^\circ\text{C}$ , which is somewhat higher than that of the sample without the Ni interlayer. Although probable nickel silicide formation is expected at the interface region prior to or during the appearance of an erbium silicide phase, no corresponding diffraction peak was detected, presumably due to the thinness of the Ni interlayer (a thickness of  $\sim 1$  nm), which is insufficient for detection via XRD. When the thickness of the Ni interlayer was increased from  $\sim 1$  to  $\sim 3$  nm in a separate experiment, a similar absence of surface defects was verified, though  $\text{ErSi}_{2-x}$  formation was largely suppressed even after annealing at  $700^\circ\text{C}$  (see Figures S1 and S2 in the Supporting Information), suggesting that the thickness of the Ni interlayer is an important parameter to be carefully optimized.

Summarizing these XRD results, it can be hypothesized that the Ni interlayer somewhat delayed the formation of erbium silicide, probably by forming an ultrathin nickel silicide layer at the interface region and interrupting Si out-diffusion to the Er film. This process is beneficial to the achievement of a subsequent growth of a uniform and smooth crystalline  $\text{ErSi}_{2-x}$  film without surface defects. Of note here is a slight shift of the  $\text{ErSi}_{2-x}(100)$  and  $\text{ErSi}_{2-x}(200)$  peaks to a low diffraction angle with the use of the Ni interlayer. For instance, the measured spacing of the  $\text{ErSi}_{2-x}(100)$  plane increased from  $0.328$  to  $0.339$  nm when the Ni interlayer was introduced. Although the origin of this volumetric expansion in an out-of-plane direction is not clear and warrants further study, it may be related to a mixing of the initially formed nickel silicide with erbium silicide, leading to the formation of an Er–Si–Ni mixture at high temperatures, as discussed in the following XPS study. Eventually, it may lead to a further stress release of the film.

A clearer picture of the Er silicidation process was obtained via the cross-sectional TEM images shown in Figure 4. For the reference sample annealed at  $500^\circ\text{C}$  (Figure 4a), two layers with an irregular interface were discriminated from the capping TaN layer and the Si substrate. Because the Si atoms make up the primary diffusing species in the Er–Si reaction system, an

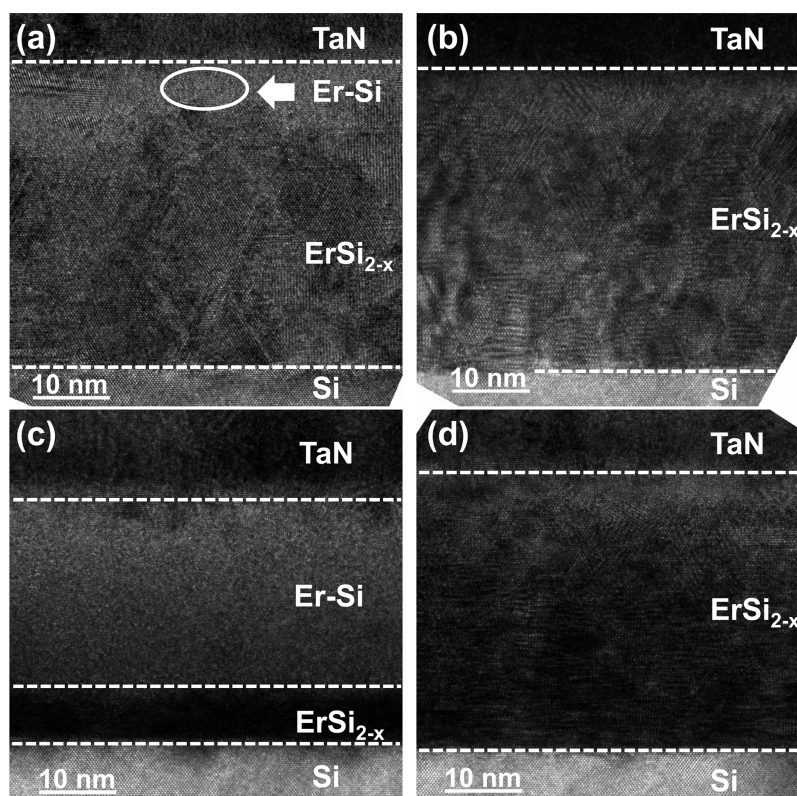


**Figure 4.** Cross-sectional TEM images of the TaN/Er/Si samples (a, b) without and (c, d) with a  $\sim 1$  nm thick Ni interlayer after annealing at different temperatures: (a, c) 500 °C and (b, d) 600 °C.

outward Si flux advances the continuous growth of an amorphous Er–Si mixed layer, while crystalline  $\text{ErSi}_{2-x}$  nucleates from the bottom region at approximately 400 °C.<sup>10,14</sup> The two discerned layers can therefore be attributed to crystalline  $\text{ErSi}_{2-x}$  and an overlying amorphous Er–Si mixture, which indicates an incomplete Er silicidation stage. A delay in the Er–Si reaction was observed in the Ni-interlayered sample considering the thinness of the  $\text{ErSi}_{2-x}$  layer compared to the reference sample at identical annealing temperatures, though a uniform interface morphology was attained in  $\text{ErSi}_{2-x}$  as shown in Figure 4c. This supports the uniform Si out-diffusion and nucleation/growth of the  $\text{ErSi}_{2-x}$  film. After annealing at 600 °C, both samples reached a near-complete silicidation stage, as shown in Figure 4b,d. These measurements are in agreement with the XRD results.

Although uniform Si out-diffusion via the early-formed interfacial layer was expected given the precedent analyses, it is still unclear whether the Ni-containing interfacial layer (primarily nickel silicide) maintains its location throughout the following erbium silicide conversion process at a higher temperature. If the formed nickel silicide remains intact at the interfacial region until the transformation of the entire quantity of Er to erbium silicide is complete, the Schottky barrier height determined by the material in direct contact with Si cannot be lowered and improvement in the electrical contact property using erbium silicide cannot be expected. Because the reverse  $J$ – $V$  characteristics can predict a possible change in the interface material in contact with Si, they were measured on samples both without and with a Ni interlayer as a function of the annealing temperature, as shown in parts a and b, respectively, of Figure 5. In addition, reverse  $J$ – $V$  characteristics of a TaN/Ni/Si sample annealed at identical temperatures were

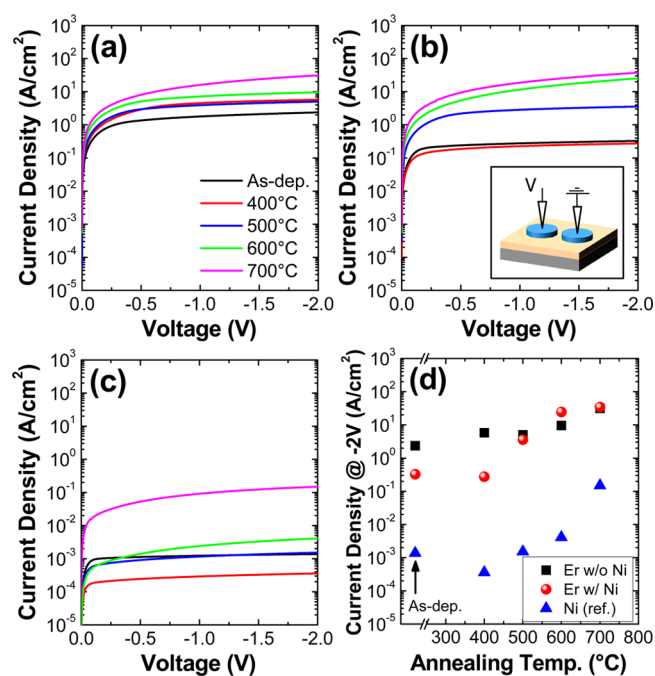


**Figure 5.** Reverse  $J$ – $V$  characteristics of the TaN/Er/n-type Si samples (a) without and (b) with a  $\sim 1$  nm thick Ni interlayer as a function of the annealing temperature. (c) shows similarly measured  $J$ – $V$  characteristics of the TaN/Ni/n-type Si sample. (d) Summarized graph showing the current densities measured at  $-2$  V for all the samples as a function of the annealing temperature. The inset of (b) is a schematic diagram showing the electrical measurement configuration.

also measured for an additional reference sample (Figure 5c). For a clearer comparison, the reverse current density measured at  $-2$  V is plotted for each sample with different annealing temperatures, as shown in Figure 5d. A large reverse current was observed for the TaN/Er/Si sample without the Ni interlayer, even without a subsequent annealing step, due to the small Schottky barrier height of Er on n-type Si.<sup>15</sup> This increased further as the transition to erbium silicide proceeded. The Ni-interlayered sample exhibited a much lower reverse current for the as-deposited state. Considering a further decrease in the current observed in the TaN/Ni/Si sample, it can be concluded that the Schottky barrier height of the as-deposited Ni-interlayered sample is dominated by Ni, which has a larger Schottky barrier height than Er.<sup>15</sup> When the annealing temperature was increased, a large increase in leakage current was observed and a current level similar to that of the TaN/Er/Si sample was achieved at 500 °C. A conversion of Er to erbium silicide was confirmed to occur at this temperature according to the XRD and TEM results; therefore, it can be assumed that the interface characteristics are dominated by an  $\text{ErSi}_{2-x}$ -to-Si contact with a low Schottky barrier height, as the erbium silicide film grows. Meanwhile, when the stacking sequence is reversed (i.e., an ultrathin Er film is used as an interlayer at the Ni/Si interface), it is reported that the interface characteristics are predominated by a NiSi-to-Si contact, independent of the Er thickness.<sup>16</sup> This emphasizes the importance of the stacking sequence to achieve a low contact resistance.

For a further understanding of the change in the Ni interlayer as a function of the annealing temperature, a series of XPS measurements were conducted following sputter etching of the surface layer. Annealing temperatures of 400 and 600 °C were chosen because the interface region adjacent to the Si substrate is suspected to be nickel silicide dominant at 400 °C and to change to an erbium silicide-rich region at 600 °C, according to the observed  $J$ - $V$  characteristics. Figure 6 illustrates the spectral changes in the Ni  $2p_{3/2}$  and Si 2p core levels after annealing at two temperatures. The spectra reflecting the chemical information on the interfacial region were selected by considering the depth profiling data of the Si 2p core level; all spectra in Figure 6 were obtained immediately prior to the intensity saturation of the Si substrate peak. A Ni  $2p_{3/2}$  peak appears at a higher binding energy ( $\sim 853.9$  eV) than that of metallic Ni ( $\sim 852.7$  eV)<sup>17,18</sup> for the sample annealed at 400 °C, as shown in Figure 6a. This implies a possible reaction between the interface Ni and the Si to form a nickel silicide phase, as expected given the  $J$ - $V$  characteristics. When the annealing temperature is low (400 °C), the average position of the Si 2p peak is located at a binding energy of  $\sim 99.5$  eV, which is nearly the same as that of the Si-Si bond from the substrate (separately measured from a reference Si wafer), as shown in Figure 6b. The binding energy of Ni-Si formed at a low temperature is reported to be close to that of Si-Si,<sup>18</sup> and also the reaction kinetics between Ni and Si prefers the formation of nickel silicide at this temperature.<sup>11,12</sup> Therefore, although there is a large contribution of the overlapping Si 2p signal originating from the underlying Si substrate, the Ni interlayer is expected to be converted to a nickel silicide phase. As the annealing temperature was increased to 600 °C, which is nearly high enough to complete the Er-Si reaction, the Ni peak shifted slightly, by  $\sim 0.2$  eV, to a lower binding energy. Although there was little observation of a notable change in the Si 2p peak, the increase in annealing temperature (600 °C)

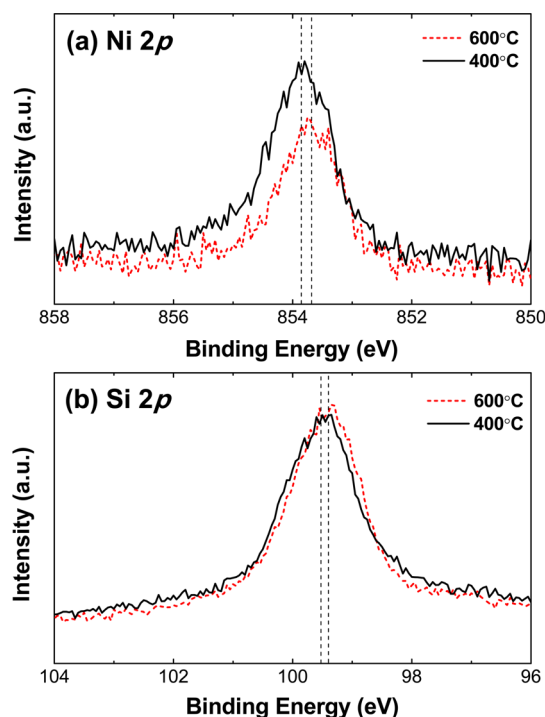


**Figure 6.** XPS core level spectra of the Ni interlayered samples annealed at 400 and 600 °C taken during depth profiling: (a) Ni  $2p$  and (b) Si  $2p$ .

caused a slight binding energy shift of the Si 2p peak to the lower binding energy side (see Figure 6b). The shift to a lower binding energy can be attributed to the lower electronegativity of Er (1.24) than that of Ni ( $\sim 1.91$ ),<sup>19</sup> which can enhance the charge transfer from Er atoms to Si-Ni bonds, as compared to Ni-Si-Ni.

Summarizing the discussed XPS analysis, it can be concluded that an ultrathin nickel silicide layer is formed at the interface region at approximately 400 °C. As the annealing temperature is increased to 600 °C, Si out-diffusion and the Er-Si reaction proceed, forming a larger volume of erbium silicide. As a result, the preformed nickel silicide is mixed with erbium silicide, and the interface region becomes erbium silicide-rich, explaining the observed increase in reverse current (Schottky barrier height lowering) to a level comparable to that found in the Er/Si sample without a Ni interlayer.

#### 4. CONCLUSION

As a facile route to prevent the formation of recessed surface defects during erbium silicidation, a Ni interlayer approximately 1 nm in thickness was inserted between TaN-capped Er and a Si substrate. While the thick TaN capping layer ( $\sim 50$  nm) prevented oxidation-induced surface defects (protruding pyramidal defects), the ultrathin Ni interlayer effectively prevented the formation of recessed defects and lessened the measured surface roughness. The interfacial Ni silicidation process occurring at a low annealing temperature (less than 400 °C) is believed to initiate the uniform nucleation/growth of subsequent Er silicidation by controlling the Si out-diffusion and to avoid the generation of recessed defects. Schottky contact behavior was observed at low annealing temperatures, and a slight increase in the formation temperature of erbium silicide was observed due to the Ni interlayer; however, a near-complete formation of erbium silicide was achieved after

annealing at 600 °C when ohmic contact behavior comparable to that of the sample without a Ni interlayer was attained, probably due to the formation of an Er–Si–Ni mixture and the subsequent enrichment of erbium silicide at the interface region in direct contact with Si.

## ■ ASSOCIATED CONTENT

### ● Supporting Information

SAM surface images and XRD spectra measured from the TaN/Er/Si samples with a Ni interlayer approximately 3 nm in thickness as a function of the annealing temperature. This material is available free of charge via the Internet at <http://pubs.acs.org/>.

## ■ AUTHOR INFORMATION

### Corresponding Author

\*E-mail: [hsubkim@skku.edu](mailto:hsubkim@skku.edu).

### Notes

The authors declare no competing financial interest.

## ■ ACKNOWLEDGMENTS

This work was supported by the IT R&D program (Grant 10039174, Technology Development of 22 nm Level Foundry Devices and PDK) of KEIT (Korea Evaluation Institute of Industrial Technology) funded by MOTIE (Ministry of Trade, Industry & Energy).

## ■ REFERENCES

- (1) Reckinger, N.; Tang, X.; Bayot, V.; Yarekha, D. A.; Dubois, E.; Godey, S.; Wallart, X.; Larrieu, G.; Łaszcz, A.; Ratajczak, J.; Jacques, P. J.; Raskin, J.-P. Low Schottky Barrier Height for ErSi<sub>2-x</sub>/n-Si Contacts Formed with a Ti Cap. *J. Appl. Phys.* **2008**, *104*, 103523.
- (2) Kuroda, R.; Tanaka, H.; Nakao, Y.; Teramoto, A.; Miyamoto, N.; Sugawa, S.; Ohmi, T. Ultra-Low Series Resistance W/ErSi<sub>2</sub>/n<sup>+</sup>-Si and W/Pd<sub>2</sub>Si/p<sup>+</sup>-Si S/D Electrodes for Advanced CMOS Platform. *IEEE Int. Electron Devices Meet., Technol. Dig.* **2010**, 580–583.
- (3) Tang, X.; Katcki, J.; Dubois, E.; Reckinger, N.; Ratajczak, J.; Larrieu, G.; Loumaye, P.; Nisole, O.; Bayot, V. Very Low Schottky Barrier to n-Type Silicon with PtEr-Stack Silicide. *Solid-State Electron.* **2003**, *47*, 2105–2111.
- (4) Wu, C. S.; Lau, S. S.; Kuech, T. F.; Liu, B. X. Surface Morphology and Electronic Properties of ErSi<sub>2</sub>. *Thin Solid Films* **1983**, *104*, 175–182.
- (5) Tsai, W. C.; Chi, K. S.; Chen, L. J. Growth of Pinhole-Free Epitaxial Yb and Er Silicide Thin Films on Atomically Clean (111) Si. *J. Appl. Phys.* **2004**, *96*, 5353–5356.
- (6) Tu, K. N.; Thompson, R. D.; Tsaur, B. Y. Low Schottky Barrier of Rare-Earth Silicide on n-Si. *Appl. Phys. Lett.* **1981**, *38*, 626–628.
- (7) Huang, W.; Ru, G. P.; Jiang, Y. L.; Qu, X. P.; Li, B. Z.; Liu, R. Improvement of Er-Silicide Formation on Si(100) by W Capping. *Thin Solid Films* **2008**, *516*, 4252–4257.
- (8) Tan, E. J.; Bouville, M.; Chi, D. Z.; Pey, K. L.; Lee, P. S.; Srolovitz, D. J.; Tung, C. H. Pyramidal Structural Defects in Erbium Silicide Thin Films. *Appl. Phys. Lett.* **2006**, *88*, 021908.
- (9) Luo, C. H.; Chen, L. J. Growth Kinetics of Amorphous Interlayers and Formation of Crystalline Silicide Phases in Ultrahigh Vacuum Deposited Polycrystalline Er and Tb Thin Films on (001)Si. *J. Appl. Phys.* **1997**, *82*, 3808–3814.
- (10) Choi, J.; Choi, S.; Kim, J.; Na, S.; Lee, H.-J.; Lee, S.-H.; Kim, H. Silicide Formation Process of Er Films with Ta and TaN Capping Layers. *ACS Appl. Mater. Interfaces* **2013**, *5*, 12744–12750.
- (11) Baglin, J. E. E.; Atwater, H. A.; Gupta, D.; d'Heurle, F. M. Radioactive Ni Tracer Study of the Nickel Silicide Growth Mechanism. *Thin Solid Films* **1982**, *93*, 255–264.
- (12) Kim, E.-H.; Forstner, H.; Foad, M.; Tam, N.; Ramamurthy, S.; Griffin, P. B.; Plummer, D. Ni<sub>2</sub>Si and NiSi Formation by Low

Temperature Soak and Spike RTPs. *RTP 2005, IEEE Int. Conf. Adv. Therm. Process. Semicond., 13th* **2005**, 177–181.

(13) Baglin, J. E.; d'Heurle, F. M.; Petersson, C. S. The Formation of Silicides from Thin Films of Some Rare-Earth Metals. *Appl. Phys. Lett.* **1980**, *36*, 594–596.

(14) Ratajczak, J.; Łaszcz, A.; Czerwinski, A.; Katcki, J.; Philipp, F.; Van Aken, P. A.; Reckinger, N.; Dubois, E. Transmission Electron Microscopy Study of Erbium Silicide Formation from Ti/Er Stack for Schottky Contact Applications. *J. Microsc.* **2010**, *237*, 379–383.

(15) Nishimura, T.; Kita, K.; Toriumi, A. Evidence for Strong Fermi-Level Pinning Due to Metal-Induced Gap States at Metal/Germanium Interface. *Appl. Phys. Lett.* **2007**, *91*, 123123.

(16) Huang, W.; Min, Y. L.; Ru, G. P.; Jiang, Y. L.; Qu, X. P.; Li, B. Z. Effect of Erbium Interlayer on Nickel Silicide Formation on Si(100). *Appl. Surf. Sci.* **2008**, *254*, 2120–2123.

(17) Moulder, J. F.; Stickle, W. F.; Soble, P. E.; Bomben, K. D. *Handbook of X-ray Photoelectron Spectroscopy*; Physical Electronics: Chanhassen, MN, 1995.

(18) Cao, Y.; Nyborg, L.; Jelvestam, U. XPS Calibration Study of Thin-Film Nickel Silicides. *Surf. Interface Anal.* **2009**, *41*, 471–483.

(19) Allred, A. L. Electronegativity Values from Thermochemical Data. *J. Inorg. Nucl. Chem.* **1961**, *17*, 215–221.

## ■ NOTE ADDED AFTER ASAP PUBLICATION

This article was published ASAP on August 14, 2014. The text of the Abstract was corrected and the revised version was reposted on August 15, 2014.